

Tuning Brønsted Acidity by up to 12 pK_a Units in a Redox-Active Nanopore Lined with Multifunctional Metal Sites

Taro J. Jones, Kaitlyn G. Dutton, Harender S. Dhattarwal, P. Thomas Blackburn, Rupak Saha, Richard C. Remsing*, and Mark C. Lipke*



Cite This: <https://doi.org/10.1021/jacs.4c15873>



Read Online

ACCESS |

Metrics & More

Article Recommendations

Supporting Information

ABSTRACT: Electrostatic interactions, hydrogen bonding, and solvation effects can alter the free energies of ionizable functional groups in proteins and other nanoporous architectures, allowing such structures to tune acid–base chemistry to support specific functions. Herein, we expand on this theme to examine how metal sites ($M = H_2, Zn^{II}, Co^{II}, Co^I$) affect the pK_a of benzoic acid guests bound in discrete porphyrin nanoprisms ($M_3\text{TriCage}$) in CD_3CN . These host–guest systems were chosen to model how porous metalloporphyrin electrocatalysts might influence H^+ transfer processes that are needed to support important electrochemical reactions (e.g., reductions of H^+ , O_2 , or CO_2). Usefully, the cavities of the host–guest complexes become hydrated at low water concentrations (10–40 mM), providing a good representation of the active sites of porous electrocatalysts in water. Under these conditions, Lewis acidic Zn^{II} and Co^{II} ions increase the Brønsted acidities of the guests by 4 and 8 pK_a units, respectively, while reduction of the Co^{II} sites to anionic Co^I sites produces an electrostatic potential that lowers acidity by ca. 4 units (8 units relative to the Co^{II} state). Lacking functional metal sites, $H_6\text{TriCage}$ increases the acidity of the guests by just 2.5 pK_a units despite the 12+ charge of this host and contributions from other factors (hydrogen bonding, hydration) that might stabilize the deprotonated guests. Thus, the metal sites have dominant effects on acid–base chemistry in the $M_3\text{TriCages}$, providing a larger pK_a range (12.75 to ≥ 24.5) for an encapsulated acid than attained via other confinement effects in proteins and artificial porous materials.

Controlling acidity in a nanoconfined environment

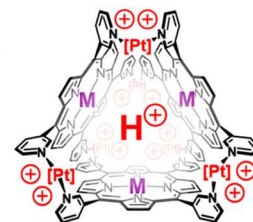
Major Influences

Redox Activity:

$M = Co^{II}/Co^I$

Lewis Acidity:

$M = Zn^{II}, Co^{II}$



Minor Influences

Electrostatics

H-Bonding

Pore Hydration

Measured pK_a values: 12.75, 14.5, 16.5, 18.2, 19.2, 20.4, ≥ 24.5

INTRODUCTION

The free energies of ions can be modified significantly by nanoconfinement (Scheme 1A),^{1–7} giving rise to important influences on acid–base chemistry in proteins^{3–5} and other 3D nanostructures.^{1,6,7} For example, proteins control solvation,³ Coulombic effects,⁴ and hydrogen bonding⁵ to stabilize or destabilize the ionized state of an acid–base pair, thereby tuning the pK_a of acidic groups^{3d,4b,5c} as needed to support functions ranging from catalysis^{4b,c,5c} to proton pumping.⁸ Strong control over acid–base chemistry has also been achieved in artificial porous structures,^{6,7} such as metal–organic nanocages,^{1,6} but these examples are often attributed primarily to Coulombic effects^{6a–f} rather than the myriad of factors that modulate acidity in proteins.^{3–5,9} Thus, in early examples from Raymond and Bergman (Scheme 1B),^{6a–c} anionic nanocages were found to favor the binding of cationic guests,^{6a} making guests easier to protonate and accelerating acid-catalyzed transformations inside these structures.^{6b,c} Likewise, Fujita^{6d} and Ward^{6e,f} have each used cationic cages to promote base-catalyzed reactivity.^{6d–f}

However, recent studies reveal more complex influences on acid–base chemistry in charged hosts. Hooley has reported enhanced acidities for ammonium cations in a positively

charged nanocage, as is expected, but non-Coulombic effects must also contribute to this behavior since the sequential protonation of 12 amines led to progressively lower pK_a values even though charge balance was maintained by anion uptake.^{6g} Gibb has also noted that the Coulombic influences of charged hosts can be modulated by hydrogen bonding, hydration, and other factors to determine the acidities of encapsulated guests.^{7b} Given the complex range of possible influences on acid–base behavior in confined microenvironments,^{3–9} there remains considerable room to better understand how hollow structures affect the free energies of protons and other charged species.

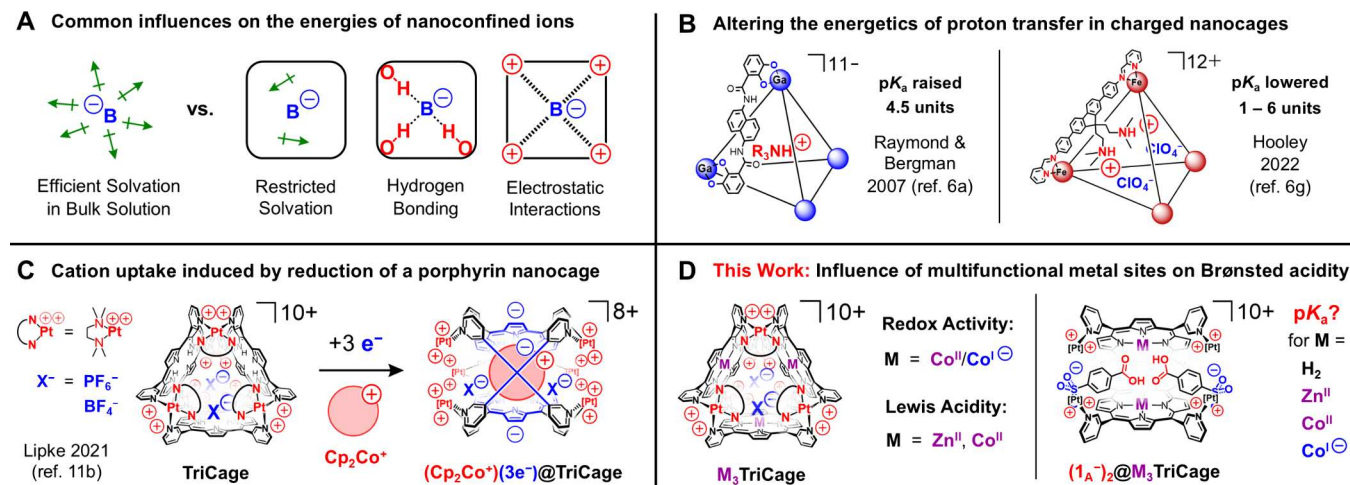
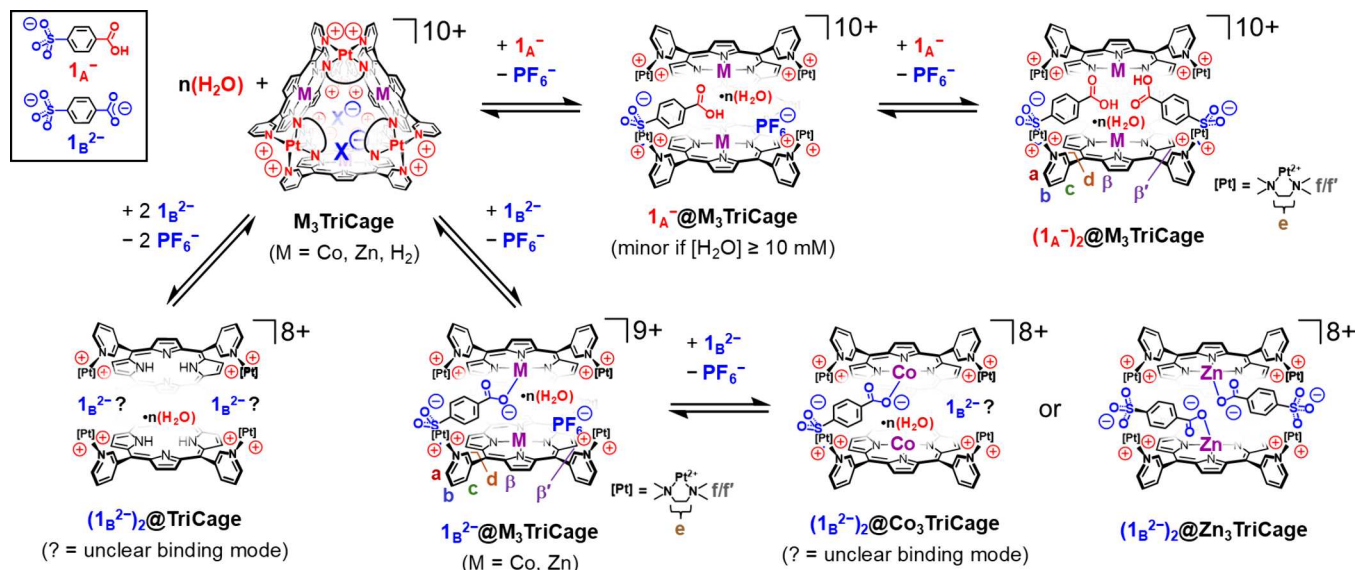
We became interested in this question in the context of redox-active porphyrin nanostructures^{10,11} that have been used as electrocatalysts for reactions such as the reduction of CO_2 or O_2 .^{12,13} A variety of metalloporphyrin nanocages¹² and

Received: November 9, 2024

Revised: December 14, 2024

Accepted: December 17, 2024

Scheme 1. Effects of Nanoconfinement on Brønsted Acidity and Other Chemistry Involving Charged Species

Scheme 2. Host-Guest Chemistry Established for Association of 1_A^- or 1_B^{2-} Inside M_3 TriCage ($M = \text{Co, Zn, H}_2$) in CD_3CN 

framework materials¹³ have been examined in this regard, but these studies have rarely addressed^{13d} how the active sites in these materials might affect charged intermediates and proton relay chains that are important for efficient turnover.¹⁴ These questions are especially vexing because redox changes will alter the distribution of charge^{11b} at the active sites during catalysis,^{13b} further complicating the confinement effects described above. Thus, we identified (tmeda)Pt-linked porphyrin nanoprisms¹¹ (M_3 TriCages, $M = \text{H}_2$, Co, Zn, Scheme 1C, D) as useful subjects for probing how protons and other ions^{11b} are affected by confinement in redox-active 3D porphyrin assemblies.

We previously reported that $\text{H}_6\text{TriCage}$ (also referred to herein as **TriCage**) binds a large cationic guest upon adding 1 e^- to each porphyrin unit (Scheme 1C),^{11b} and we hypothesized that similar electrostatic effects might be seen upon reduction of $\text{Co}_3\text{TriCage}$ to its zwitterionic *tris*- Co^{I} state.^{11c} To measure the impact on proton transfer equilibria, the anion-binding ability of the TriCages was used to install two 4-sulfanatobenzoic acid guests (1_A^- , Scheme 1D) in each cage, following our observation that *p*-toluenesulfonate (2^-) binds strongly in **TriCage** ($K_a \approx 10^{7.5} \text{ M}^{-1}$ in CD_3CN).^{11d}

Remarkably, the resulting complexes have acidities that are varied across a larger pK_a range (12.75 to ≥ 24.5 in CD_3CN) than those achieved in proteins and other nanocages,^{3–9,15} even though Coulombic effects, hydrogen bonding, and hydration have only small to moderate influences on acidities in the TriCages. Instead, as described herein, the redox-active and/or Lewis acidic Co and Zn sites have dominant effects on increasing or decreasing the acidities of the guests, revealing the unique influences of these metalloporphyrin nanocages on acid–base chemistry.

RESULTS AND DISCUSSION

Complexation of Acid/Base Functionalized Guests.

¹H NMR spectroscopy was used to examine the encapsulation of 4-sulfanatobenzoic acid (1_A^-) and its conjugate base 4-sulfanatobenzoate (1_B^{2-}) by the TriCages in CD_3CN (Scheme 2). For all three M_3 TriCage derivatives, addition of 2 equiv 1_A^- (as its TBA⁺ salt) resulted in disappearance of the signals of the empty host and appearance of a new set of signals corresponding to a 1:2 host–guest complex (Figures 1, S27, and S39). ESI(+)–HRMS further confirmed the formation of

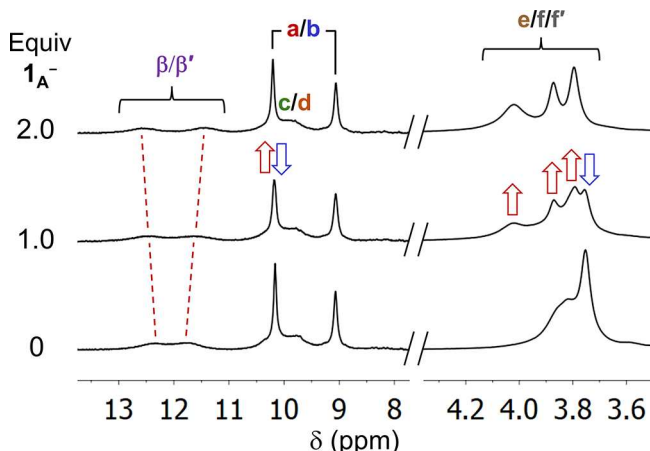


Figure 1. Truncated ^1H NMR spectra (500 MHz, CD_3CN , 25 °C) acquired during addition of 1A^- to $\text{Co}_3\text{TriCage}$. Note that labels of signals correspond to those indicated in **Scheme 2**, and different scaling is used in each region of the spectra displayed.

$(1\text{A}^-)_2@\text{TriCage}$ and $(1\text{A}^-)_2@\text{Co}_3\text{TriCage}$ (**Figures S61 and S64**). However, the latter mass spectrum indicated partial deprotonation of the bound guests, and attempts to observe $(1\text{A}^-)_2@\text{Zn}_3\text{TriCage}$ showed only the doubly deprotonated complex $(1\text{B}^{2-})_2@\text{Zn}_3\text{TriCage}$, providing an early indication that the acidity of 1A^- is enhanced in the metallated derivatives of **TriCage** (*vide infra*).

Quantitative binding of 1A^- in the **TriCages** is consistent with the strong 1:2 association of 2^- in **TriCage**. However, while 2^- binds noncooperatively, 1A^- associates with positive cooperativity. Hence, an equimolar mixture of 1A^- and **Co₃TriCage** displays an NMR spectrum consistent with the empty host combined in equal amounts with the 1:2 complex (**Figure 1**). Likewise, titration of **TriCage** and $\text{Zn}_3\text{TriCage}$ with 1A^- results in direct conversion of these hosts to their 1:2 complexes, with only small signals potentially corresponding to a 1:1 complex observed during the experiment (**Figures S28 and S40**). Mass spectrometry of a 1:1 mixture of **TriCage** and 1A^- (**Figure S62**) also supports the cooperativity of guest binding, showing the 1:1 complex as a minor component (~8%) of the sample relative to the empty host and 1:2 complex. The cooperative binding of 1A^- was initially attributed to hydrogen-bonding between the guests, but as

discussed below, traces of water were found to promote this cooperativity, suggesting that more complex factors underly this behavior.

In contrast to 1A^- , the deprotonated guest 1B^{2-} shows considerable variation in its interactions with the different $\text{M}_3\text{TriCage}$ derivatives. Addition of 1 equiv 1B^{2-} to **Co₃TriCage** resulted in complete disappearance of the ^1H NMR signals of the empty host, and the appearance of several new signals that were shifted considerably from those of **Co₃TriCage** (**Figure 2A**). Most notably, the two porphyrin β CH resonances are split into three similarly sized groups of broad signals, one group resembling those of the empty host (δ 11–13 ppm) while two others are shifted downfield to ranges of δ 13.8–15.8 and 16.6–19.9 ppm. These latter signals are reminiscent of how the β CH signals appear when simple benzoate anions coordinate to the cobalt sites of **Co₃TriCage**,^{11e} suggesting 1B^{2-} engages in similar interactions inside this host. The approximately equal sizes of the groups of β CH signals indicate that the carboxylate end of 1B^{2-} coordinates to two of the cobalt centers in the host, either simultaneously via a bridging interaction or by fast exchange between the two cobalt ions.

Resonances of the pyridyl groups and tmeda ligands of **Co₃TriCage** are also split to varying extents upon binding 1B^{2-} . The tmeda region of the spectrum, in particular, shows several signals, two of which are shifted downfield by >1 ppm from those of the empty host. The considerable desymmetrization of the spectrum of $1\text{B}^{2-}@\text{Co}_3\text{TriCage}$ suggests that 1B^{2-} cannot reposition itself freely in this host (aside from possible exchange of the carboxylate group between two Co^{II} sites). These findings are consistent with rigid binding enforced by an $\text{ArCO}_2^- \rightarrow \text{Co}^{\text{II}}$ interaction. However, the host does not appear to support more than one such interaction despite possessing three Co^{II} sites. Thus, adding a second equivalent of 1B^{2-} to $1\text{B}^{2-}@\text{Co}_3\text{TriCage}$ results in partial precipitation of the complex from solution and broadening of its NMR signals without changing their chemical shifts (**Figure S23**). These observations suggest against strong association of the second 1B^{2-} guest, presumably because electrostatic repulsion prevents two CO_2^- groups from binding near the center of the cage. Consistent with weak binding of the second 1B^{2-} guest, we were unable to observe a 1:2 complex by ESI(+)·HRMS.

Guest 1B^{2-} also shows negative cooperativity for association in $\text{Zn}_3\text{TriCage}$, but the higher Lewis acidity^{11e,16} of Zn^{II}

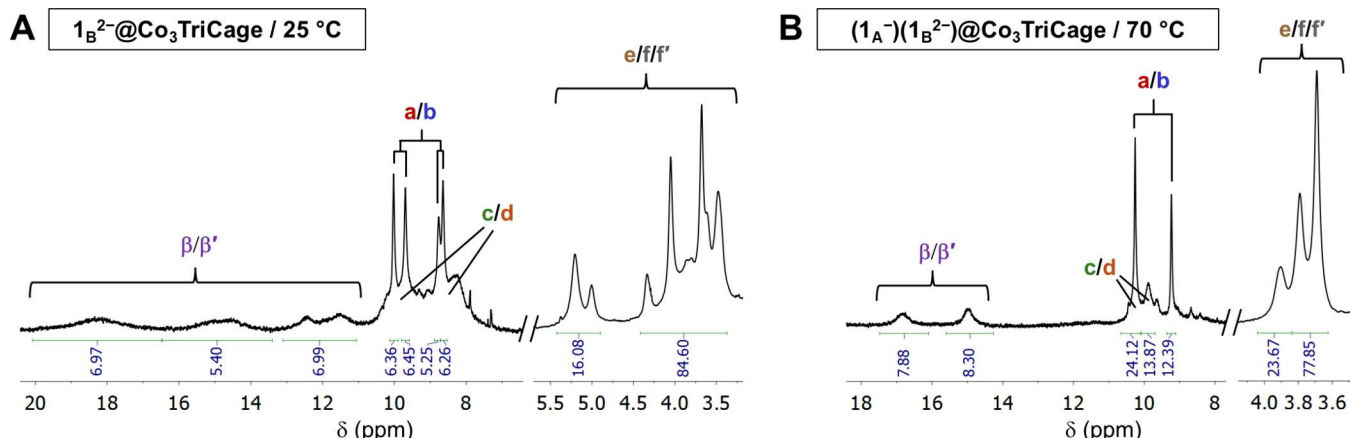


Figure 2. (A) Truncated ^1H NMR spectrum (500 MHz, CD_3CN) of $1\text{B}^{2-}@\text{Co}_3\text{TriCage}$ recorded at 25 °C. (B) Truncated ^1H NMR spectrum (500 MHz, CD_3CN) of $(1\text{A}^-)(1\text{B}^{2-})@\text{Co}_3\text{TriCage}$ recorded at 70 °C. Labels of signals correspond to those in **Schemes 2 and 3**.

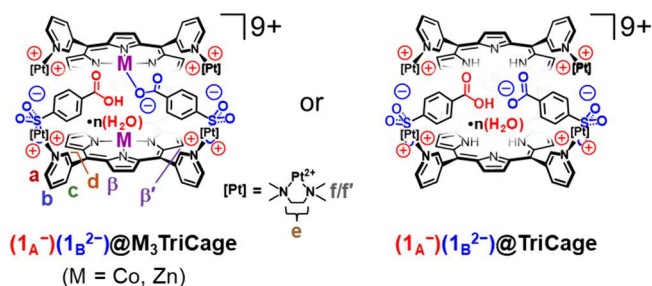
reinforces binding of this guest enough to enable clear identification of both a 1:1 and 1:2 complex by ^1H NMR spectroscopy (Figures S48 and S50) and ESI(+)·HRMS (Figures S67 and S68). The 1:1 complex is formed quantitatively upon adding 1 equiv of 1_{B}^{2-} to $\text{Zn}_3\text{TriCage}$, producing an NMR spectrum (Figure S48) in which most of the aromatic resonances of the cage are split into two distinct signals of equal size, suggesting loss of mirror symmetry between the two triangular faces. Most of the aromatic signals are well-defined, but the 2-position CH resonance of the pyridyl groups is broadened and only one such signal is seen, corresponding to just half of these CH positions. Heating the sample to 60 °C led to the appearance of the missing 2-position signal and considerable sharpening of the other signals of the host (Figure S49), yielding a spectrum that clearly corresponds to a structure with time-averaged C_3 symmetry. Conversely, cooling to −40 °C produced an NMR spectrum consistent with a low symmetry structure (Figure S49).

A detailed analysis is impractical for the many broad and overlapping signals in the low-temperature spectrum of $1_{\text{B}}^{2-}@\text{Zn}_3\text{TriCage}$, but insights were gained by comparison with the spectrum acquired at 25 °C for the 1:2 complex $(1_{\text{B}}^{2-})_2@\text{Zn}_3\text{TriCage}$ (Figures S50, S51). The latter spectrum is also complicated, but nearly every aromatic peak is sharp, allowing confident assignment of C_2 symmetry based on minimum integrals of 2H for signals in this region. This symmetry implies that two of the Zn^{II} sites are equivalent, and thus, both guests must coordinate to zinc centers. Notably, distinct signals near 7.25 and 9.75 ppm in the spectrum of the 1:2 complex match similar resonances in the low temperature spectrum of the 1:1 complex (Figure S51). Likewise, both spectra display broad resonances for the guest between 6–6.5 ppm, suggesting 1_{B}^{2-} has a similar binding mode in both the 1:1 and 1:2 complexes.

Interactions of 1_{B}^{2-} with **TriCage** differ significantly from those of this guest with the metalated hosts. The ^1H NMR spectrum of **TriCage** is only slightly altered after adding 0.5 equiv of 1_{B}^{2-} (Figure S37), but further additions broaden and shift the signals of the host until ≥ 1.5 equiv 1_{B}^{2-} have been added, at which point some resonances partially resharpen. These observations suggest that two 1_{B}^{2-} guests bind cooperatively in **TriCage** and that the resulting complex engages in fast exchange with the empty host on the NMR time scale. However, definitive interpretation of the mode of binding is hindered because many signals remain broad after 2 equiv 1_{B}^{2-} have been added, at which point the complex begins to precipitate. Furthermore, small additional signals are observed that presumably correspond to other modes of interaction between 1_{B}^{2-} and **TriCage** (Figure S35, S36), but the nature of these interactions could not be determined. Despite these limitations, it can be concluded that 1_{B}^{2-} associates with **TriCage** and that these interactions differ from those with the metalated hosts. A 1:2 binding stoichiometry appears likely but is not certain since only a 1:1 complex $1_{\text{B}}^{2-}@\text{TriCage}$ was observable by ESI(+)·HRMS (Figure S63).

Host–guest complexes containing one equivalent each of 1_{A}^- and 1_{B}^{2-} (1:1:1 complexes, Scheme 3) were also characterized. The complex $(1_{\text{A}}^-)(1_{\text{B}}^{2-})@\text{Co}_3\text{TriCage}$ has a ^1H NMR spectrum resembling that of $(1_{\text{A}}^-)_2@\text{Co}_3\text{TriCage}$ except that the β CH signals are so broadened for the 1:1:1 complex as to barely be identifiable (Figure S16). Heating to 70 °C led to the resolution of these signals into two broad resonances centered near 14.97 and 16.83 ppm (Figure 2B).

Scheme 3. Complexes of the Mixed-Protonation-State Guests 1_{A}^- and 1_{B}^{2-} in $\text{M}_3\text{TriCage}$ ($\text{M} = \text{Co}, \text{Zn}, \text{H}_2$)



These downfield chemical shifts suggest that 1_{B}^{2-} coordinates to cobalt, and the observation of just two β CH signals indicates that the carboxylate group exchanges rapidly among the three Co^{II} sites at 70 °C. Other regions of the spectrum also indicate high symmetry ($D_{3\text{h}}$), suggesting that the two guests readily exchange between which is protonated and which is coordinated to cobalt. In addition to NMR characterization, $(1_{\text{A}}^-)(1_{\text{B}}^{2-})@\text{Co}_3\text{TriCage}$ was also observed by ESI(+)·HRMS (Figure S65).

Formation of $(1_{\text{A}}^-)(1_{\text{B}}^{2-})@\text{Zn}_3\text{TriCage}$ was investigated by adding an equivalent of 1_{A}^- to $1_{\text{B}}^{2-}@\text{Zn}_3\text{TriCage}$, producing a ^1H NMR spectrum reminiscent of those of the other complexes, but with multiple overlapping features observed for the signals of the host (Figure S46). Additionally, no resonance can be discerned for the pyridyl 2-position CH bonds that face the interior of the cage. The missing and poorly defined signals suggest that multiple conformations of the 1:1:1 complex form and exchange slowly on the NMR time scale. The signals of the complex are much better defined at 70 °C (Figure S47), but the spectrum remains complex, suggesting that rearrangements of the two guests still do not occur quickly on the NMR time scale. Strong coordination of 1_{B}^{2-} to zinc is likely responsible for the slower dynamics of this complex relative to its Co^{II} counterpart.

Lastly, unmetalated **TriCage** binds 1_{A}^- and 1_{B}^{2-} to reveal an NMR spectrum (Figure S32) with features resembling those of its 1:2 complex with 1_{A}^- , except for two signals that are broadened or missing: no signal is seen for the inward-facing pyridyl CH bonds, and significant broadening occurs for the resonance(s) of the porphyrin β CH positions facing the apertures of the cage. This latter signal is somewhat better resolved at 70 °C (Figure S33), yielding a spectrum that would be consistent with $D_{3\text{h}}$ symmetry if not for the missing pyridyl CH resonance. Since the chemical shift of these pyridyl CH bonds is highly influenced by guests, and the separation between two NMR resonances affects their coalescence,¹⁷ it is plausible that the sulfonate groups exchange too slowly between binding sites to average these CH signals, while the rest of the spectrum corresponds to higher symmetry. It is conceivable that repositioning of guests in $(1_{\text{A}}^-)(1_{\text{B}}^{2-})@\text{TriCage}$ is slowed by CO_2^- – HO_2C interactions that prevent the guests from moving independently.

The host–guest complexes described above provide useful subjects for studying confinement effects on acidity. Thus, it is useful to highlight key observations regarding these complexes: (1) All three cages bind 1_{A}^- with positive cooperativity to yield 1:2 host–guest complexes. The CO_2H resonance could not be identified for these complexes, but upfield shifts of the CH signals of the guests (Figures S39–S43) suggest the guests sit deep inside each host.¹⁸ (2) Guest 1_{B}^{2-} binds with negative

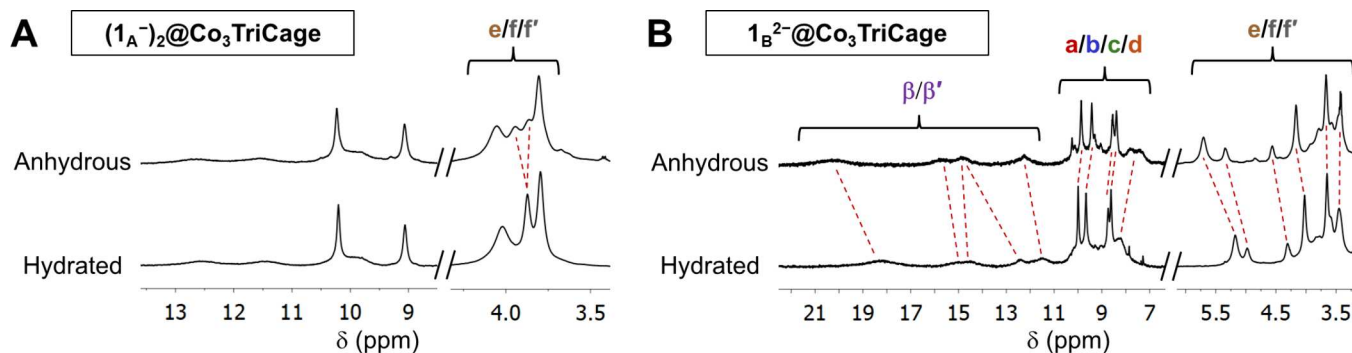


Figure 3. ^1H NMR spectra (500 MHz, CD_3CN , 25 °C) of the hydrated vs anhydrous states of (A) $(1_{\text{A}}^-)_2@\text{Co}_3\text{TriCage}$ showing changes to its tmeda resonances; and (B) $1_{\text{B}}^{2-}@\text{Co}_3\text{TriCage}$ showing changes to nearly all signals of the complex.

cooperativity in the Co_3 and Zn_3 cages, forming 1:1 complexes in which the CO_2^- group coordinates to a metal site. This interaction is also seen for a second 1_{B}^{2-} guest binding in the Zn_3 host, while the Co_3 derivative supports only one such interaction. Association of 1_{B}^{2-} with TriCage shows that metal sites are not essential for binding this guest. (3) All three cages form 1:1:1 complexes with the guests in their mixed protonation states 1_{A}^- and 1_{B}^{2-} . Carboxylate-metal coordination is seen for these complexes in the metalated hosts, while hydrogen bonding between the guests likely occurs in $(1_{\text{A}}^-)(1_{\text{B}}^{2-})@\text{TriCage}$.

Hydration of the Host–Guest Complexes. Solvation often has a profound influence on acid–base chemistry,^{3b,6h,7b,19} so it is notable that water associates readily with most of the complexes described in the previous section. Association of water is evident from differences in the ^1H NMR spectra of $(1_{\text{A}}^-)_2@\text{M}_3\text{TriCage}$ ($\text{M} = \text{Co, Zn, H}_2$) acquired in anhydrous CD_3CN vs solvent that has absorbed ambient moisture (the latter being the conditions used in the previous section). For example, differences are seen in the signals of the tmeda ligands of $(1_{\text{A}}^-)_2@\text{Co}_3\text{TriCage}$ in wet vs dry conditions (Figure 3A), whereas the spectrum of empty $\text{Co}_3\text{TriCage}$ is unaffected. Titration of an anhydrous solution of $(1_{\text{A}}^-)_2@\text{Co}_3\text{TriCage}$ (1 mM) with water resulted in conversion between the dry and hydrated presentations of the ^1H NMR spectrum by the time 10 equiv H_2O (10 mM) had been added (Figure S15), suggesting fairly strong interaction of water with the complex.

Complexes of 1_{A}^- with TriCage and $\text{Zn}_3\text{TriCage}$ also showed the influence of water on host–guest interactions. Several signals of $(1_{\text{A}}^-)_2@\text{TriCage}$ were shifted and/or broadened in the absence of water, especially the porphyrin NH resonance and signals of the host arising from aromatic CH bonds nearest to its apertures (Figures S29, S30). Furthermore, signals consistent with formation of a 1:1 complex were observed to appear and disappear up titration of 1_{A}^- into an anhydrous solution of TriCage (Figure S31). Similar observations were made for interactions of 1_{A}^- with anhydrous samples of $\text{Zn}_3\text{TriCage}$ (Figures S44 and S45), and thus, it appears that hydration of the pore is needed to promote cooperative association of 1_{A}^- in the TriCages . This is an interesting finding since aqueous solvation ordinarily weakens the dimerization of carboxylic acids. Apparently, the constraints of the nanocavity make it more favorable for the CO_2H groups to hydrogen bond with water rather than directly with each other. In comparison, the p -tolyl SO_3^- guests

in $(2^-)_2@\text{TriCage}$ ^{11d} were found to induce much weaker interactions with water (Figure S60).

The ^1H NMR spectrum of $1_{\text{B}}^{2-}@\text{Co}_3\text{TriCage}$ also differs significantly between anhydrous and wet conditions. The most downfield β CH signal is shifted by approximately +2 ppm in the absence of water (Figure 3B), and likewise, the most downfield signal of the tmeda ligand is found over 0.5 ppm more downfield under anhydrous conditions. Nearly full conversion between the dry and hydrated states was achieved upon titration with 40 equiv H_2O (40 mM, Figure S26), revealing that the confined environment in this complex hydrates less readily than the protonated state.

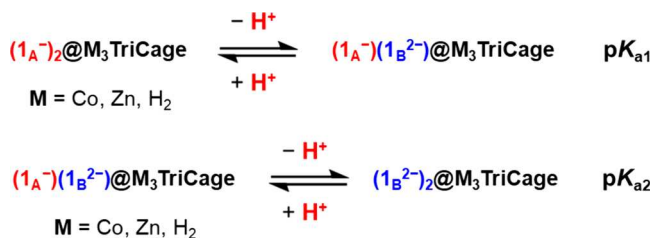
This observation is notable since water, being a highly polar solvent, usually stabilizes the ionic state of an acid–base pair,^{19c} but in the confines of $\text{Co}_3\text{TriCage}$, water appears to interact less strongly with the deprotonated carboxylate guest 1_{B}^{2-} than with its conjugate acid. The effects of water on interactions between 1_{B}^{2-} and TriCage were also tested, finding that complexation is weaker under anhydrous conditions,²⁰ leading to greater precipitation of the host when 1_{B}^{2-} was added (Figure S38). Lastly, the ^1H NMR signal of water is broadened and shifted upfield by the 1:1 complex between $\text{Zn}_3\text{TriCage}$ and 1_{B}^{2-} but not by the 1:2 complex or empty host (Figure S52), suggesting that only the 1:1 complex is easily hydrated.

Interestingly, moisture barely affects the ^1H NMR spectrum of $(1_{\text{A}}^-)(1_{\text{B}}^{2-})@\text{Co}_3\text{TriCage}$ at 25 °C, though slight differences in chemical shifts are seen for the β CH signals under wet vs dry conditions at 70 °C, suggesting some degree of hydration of the complex (Figure S21). Because changes to the spectrum are so subtle at 25 °C, it was difficult to directly evaluate how readily hydration occurs. However, as described in the next section, acid–base titration experiments revealed that water affects host–guest speciation in a way that indicates hydration is weaker for the 1:1:1 complex than for $1_{\text{B}}^{2-}@\text{Co}_3\text{TriCage}$ and $(1_{\text{A}}^-)_2@\text{Co}_3\text{TriCage}$. Hydrogen-bond donation from the protonated guest to its conjugate base^{19b,21} may be responsible for weakening interactions of the guests with water in the 1:1:1 complex. Interestingly, the different interactions of these complexes with water yield unexpected ways that hydration affects the acidities of the guests (see below), but since the strength of these effects is ultimately rather small ($\Delta\text{p}K_{\text{a}} \leq 0.5$), a more detailed analysis of interactions of water with the host–guest complexes was not pursued.

Acidity of Encapsulated Carboxylic Acids. Titration experiments were performed to measure the acidities of the 1:2

complexes of 1_A^- with the different TriCage derivatives in MeCN (Scheme 4). Each complex was titrated with a neutral

Scheme 4. Deprotonations of $(1_A^-)_2@M_3\text{TriCage}$



N-donor base^{19a} that was approximately matched in strength to the acidity of the host–guest complex, allowing the determination of the pK_a of the encapsulated guests (Table 1, Figures S73–S82) based on the known acidities of the

Table 1. Acidities Host-Guest Complexes of 1_A^-

Acid	pK_{a1} in MeCN ^a (in dry MeCN)	pK_{a2} in MeCN ^a
1_A^-	20.75 ± 0.04^b	N/A
$(1_A^-)_2@Co_3\text{TriCage}$	16.53 ± 0.06^c ($\sim 16.2^d$)	19.21 ± 0.04^e
$1_A^-@Co_3\text{TriCage}$	$\leq 16.0 \pm 0.15^f$	N/A
	($\geq 16.5^g$)	
$1_A^-@Co^I_3\text{TriCage}$	($\geq 24.5^h$)	N/A
$(1_A^-)_2@TriCage$	18.2 ± 0.1^e	20.4 ± 0.1^b
$(1_A^-)_2@Zn_3\text{TriCage}$	12.75 ± 0.07^i	$\sim 14.5^j$

^aExcept where noted, pK_a values are the mean \pm est. std. error of three acid–base titrations performed in CD_3CN containing ambient moisture (typically 50–100 mM water). ^bMeasured with N,N,N',N' -tetramethyl-1,3-butanediamine. ^cMeasured with Et_2BnN . ^dFrom two titrations with Et_2BnN in dry CD_3CN . ^eMeasured with Et_3N . ^fEstimated from the equilibrium $(1_A^-)_2@Co_3\text{TriCage} + Co_3\text{TriCage} + 2 R_3N \rightleftharpoons 2 1_B^{2-}@Co_3\text{TriCage} + 2 R_3NH^+$. ^gEstimated using pK_{a1} of the diprotic complex under anhydrous conditions as the lower bound of K_{eff} for the equilibrium in caption f. ^hFrom cyclic voltammetry measured on the complex $1_B^{2-}@Co_3\text{TriCage}$. ⁱMeasured with 2,6-lutidine, and ^j2,4,6-collidine.

protonated titrants. Because hydrated conditions are more relevant to possible electrocatalytic applications,^{12,13} these studies were performed in solvent containing traces of water sufficient to fully hydrate the host–guest complexes. Note that traces of water might stabilize the conjugate acids of the titrants by small amounts,^{19a,c} potentially affecting the equilibria for deprotonating the encapsulated guests. However, this effect is of minor significance for comparing the host–guest complexes since large differences in pK_a were found between the complexes, these measurements showed good reproducibility, and water should have similar effects on all the bases employed.^{19c}

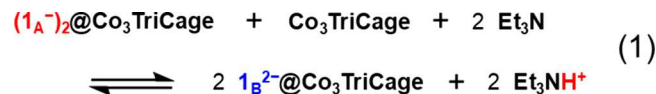
Titration of $(1_A^-)_2@Co_3\text{TriCage}$ with Et_2BnN resulted in nearly complete conversion of the diprotic complex to its monoprotic state $(1_A^-)(1_B^{2-})@Co_3\text{TriCage}$ after 4 equiv of the amine had been added (Figure S75). These measurements revealed a pK_{a1} of 16.53 ± 0.06 for the diprotic complex, representing more than a 10,000-fold increase in acidity relative to that measured for the TBA^+ salt of 1_A^- in MeCN ($pK_a = 20.75 \pm 0.04$).^{22,23} The increased acidity of the encapsulated guest can be attributed to stabilization of its conjugate base 1_B^{2-} by the positive charge of the host, by

hydrogen-bonding with the remaining protonated guest, and/or by coordination of CO_2^- to cobalt.^{11e} This latter interaction is estimated to stabilize 1_B^{2-} by at least 2.25 kcal mol⁻¹ since the unmetalated complex $(1_A^-)_2@TriCage$ was less acidic by 1.7 pK_a units ($pK_{a1} = 18.2 \pm 0.1$). Conversely, a much higher acidity was measured for the first deprotonation of $(1_A^-)_2@Zn_3\text{TriCage}$ ($pK_{a1} = 12.75 \pm 0.07$), reflecting the greater Lewis acidity of Zn^{II} versus Co^{II} .^{11e}

In all three hosts, the second 1_A^- guest was more difficult to deprotonate than the first, though only by moderate amounts, with the smallest change in acidity measured for $(1_A^-)(1_B^{2-})@Zn_3\text{TriCage}$ ($pK_{a2} \approx 14.5$, $\Delta pK_{a1,2} \approx 1.75$). The high acidity maintained in this monoprotic complex indicates that, upon deprotonation, both guests coordinate to the zinc sites in $(1_B^{2-})_2@Zn_3\text{TriCage}$. This necessarily places both CO_2^- groups near the center of the cage, so it is interesting that acidity is not decreased more by the electrostatic repulsion⁴ of these groups. Apparently, the Zn^{II} sites are electron withdrawing enough to prevent anion–anion repulsion and $CO_2H \cdots O_2C$ hydrogen bonding from having very large effects on the acidity of the monoprotic state. In contrast, $(1_A^-)(1_B^{2-})@Co_3\text{TriCage}$ has a pK_{a2} (19.21 ± 0.04) that is raised by a larger amount relative to the diprotic state ($\Delta pK_{a1,2} = 2.67$), consistent with the inability of the second 1_B^{2-} guest to coordinate to cobalt (see above).

The unmetalated complex $(1_A^-)(1_B^{2-})@TriCage$ also has an acidity ($pK_a = 20.4 \pm 0.1$) that is more than 2 orders of magnitude lower than that of its diprotic state ($\Delta pK_{a1,2} = 2.2$). This decrease can be attributed to $1_B^{2-} \cdots 1_A^-$ interactions that stabilize the monoprotic state of the complex and which should be maximized in the absence of metal sites for 1_B^{2-} to coordinate to. Indeed, the lower acidity of $(1_A^-)(1_B^{2-})@TriCage$ relative to $(1_A^-)(1_B^{2-})@Co_3\text{TriCage}$ can be attributed to stronger guest–guest interactions in the former. Note, however, that these analyses ultimately suggest that interactions between 1_B^{2-} and 1_A^- are weak even in the unmetalated complex, representing a stabilization of only ~ 1.5 kcal mol⁻¹ if it is assumed that the guest–guest interactions increase the acidity of the diprotic state by as much as the acidity of the monoprotic state is decreased. Even if this assumption does not hold, it can still be concluded that $1_B^{2-} \cdots 1_A^-$ interactions are weaker than $1_B^{2-} \cdots Co^{II}$ coordination, hence the lower acidities for the complexes of the unmetalated host.

Additional experiments were performed to probe how guest–guest interactions affect the acidity of the 1:2 complex $(1_A^-)_2@Co_3\text{TriCage}$. An equimolar mixture of this complex and $Co_3\text{TriCage}$ was titrated with Et_3N , resulting in the formation of the 1:1 complex $1_B^{2-}@Co_3\text{TriCage}$ (eq 1) with



little of the 1:1:1 complex $(1_A^-)(1_B^{2-})@Co_3\text{TriCage}$ detected by NMR spectroscopy during the experiment (Figure S77). This latter observation implies that cooperative binding of the two guests in $(1_A^-)_2@Co_3\text{TriCage}$ must be more favorable than in $(1_A^-)(1_B^{2-})@Co_3\text{TriCage}$. The deprotonation of the 1:2 complex in the presence of empty host was fitted to a simple acid–base equilibrium to give an effective $pK_{a(Eff)}$ of 16.8 ± 0.15 , and this value was deconvoluted into contributions from formation of the 1:1 complex $1_A^-@$

$\text{Co}_3\text{TriCage}$ followed by the equilibrium for deprotonating this complex (Figure S77). A K of ≤ 0.0075 can be estimated for the first of these equilibria based on HRMS data for a 1:1 mixture of 1_{A}^- and TriCage (Figure S62), implying a $\text{p}K_{\text{a}} \leq 16.0 \pm 0.15$ for deprotonation of $1_{\text{A}}^- @ \text{Co}_3\text{TriCage}$. Thus, even based on the upper bound of this $\text{p}K_{\text{a}}$ estimate, the 1:1 complex of 1_{A}^- in $\text{Co}_3\text{TriCage}$ appears to be more acidic than the corresponding 1:2 complex.²⁴

Lastly, titrations of $(1_{\text{A}}^-)_2 @ \text{Co}_3\text{TriCage}$ with Et_2BnN were performed under anhydrous conditions, revealing a $\text{p}K_{\text{a}} (\sim 16.2)$ that is just slightly lower than that measured in the hydrated complexes.²⁵ Interestingly, titration of Et_2BnN into an equimolar mixture of 1_{A}^- and $\text{Co}_3\text{TriCage}$ in dry CD_3CN produced $(1_{\text{A}}^-)(1_{\text{B}}^{2-}) @ \text{Co}_3\text{TriCage}$ as the only deprotonated complex formed, reversing the behavior seen in wet solvent. This finding indicates that water must stabilize $(1_{\text{A}}^-)_2 @ \text{Co}_3\text{TriCage}$ and $1_{\text{B}}^{2-} @ \text{Co}_3\text{TriCage}$ relative to $(1_{\text{A}}^-)(1_{\text{B}}^{2-}) @ \text{Co}_3\text{TriCage}$, implying that the 1:1:1 complex has the weakest interactions with water.

Taken together, the above findings reveal subtle counter-intuitive effects of hydration and guest–guest interactions on the acidity of 1_{A}^- bound in $\text{Co}_3\text{TriCage}$. In particular, the 1:2 complex $(1_{\text{A}}^-)_2 @ \text{Co}_3\text{TriCage}$ is stabilized by cooperative interactions between water and the two 1_{A}^- guests, producing a somewhat lower acidity than that of the 1:1 complex $1_{\text{A}}^- @ \text{Co}_3\text{TriCage}$ under comparable conditions. Water and $\text{CO}_2\text{H} \cdots \text{O}_2\text{C}$ interactions both can increase the acidities of carboxylic acids in bulk MeCN ,^{19,21} so it is interesting that hydration and guest–guest interactions combine to produce the opposite effect in $(1_{\text{A}}^-)_2 @ \text{Co}_3\text{TriCage}$. In the absence of water, however, the estimated acidity of the 1:1 complex ($\text{p}K_{\text{a}} \geq 16.5$) is lower than that of the 1:2 complex, consistent with the favorable $1_{\text{B}}^{2-} \cdots 1_{\text{A}}^-$ interactions expected upon deprotonation of the latter.²¹

Effects of Pore Reduction on Acidity. Cyclic voltammetry was used to measure the $\text{Co}^{\text{II}}/\text{Co}^{\text{I}}$ reduction potentials of the complexes of 1_{A}^- and 1_{B}^{2-} in $\text{Co}_3\text{TriCage}$, allowing the acidities of the reduced states of these complexes to be calculated.²⁶ The 1:2 complex of 1_{A}^- shows a single broadened $3 \text{ e}^- \text{ Co}^{\text{II}/\text{I}}$ redox couple centered at -1.03 V vs $\text{Fc}^{+/\text{0}}$ (Figure 4A), which is just 50 mV negative of the corresponding $\text{Co}^{\text{II}/\text{I}}$ reduction of $\text{Co}_3\text{TriCage}$.^{11c} The deprotonated 1:1 complex $1_{\text{B}}^{2-} @ \text{Co}_3\text{TriCage}$ exhibits a similar reversible reduction ($E_{1/2} = -1.00 \text{ V}$) but also a smaller quasireversible redox couple at $E_{1/2} = -1.47 \text{ V}$ (Figure 4B). The more positive feature is assigned to the $\text{Co}^{\text{II}}/\text{Co}^{\text{I}}$ reduction of the two free Co^{II} centers while the more negative feature corresponds to the Co^{II} site that coordinates 1_{B}^{2-} (Scheme 5). The 470 mV cathodic shift of this reduction indicates that the carboxylate group stabilizes the Co^{II} state by nearly 11 kcal mol^{-1} , representing a stronger stabilization than would be expected based on the $\text{CO}_2^- \rightarrow \text{Co}^{\text{II}}$ interaction ($\sim 4 \text{ kcal mol}^{-1}$) in the *tris*- Co^{II} state of host–guest complex.²⁷ The $\sim 7 \text{ kcal mol}^{-1}$ difference can be attributed to the destabilization of the anionic carboxylate group by unfavorable electrostatic interactions with the three anionic Co^{I} sites in the reduced zwitterionic state of the host.

The destabilization of 1_{B}^{2-} in $1_{\text{B}}^{2-} @ \text{Co}_3\text{TriCage}$ corresponds to an increase in the $\text{p}K_{\text{a}}$ of $1_{\text{A}}^- @ \text{Co}_3\text{TriCage}$ by 8 units relative to that of the *tris*- Co^{II} state, revealing a $\text{p}K_{\text{a}} \geq 24.5$ for 1_{A}^- when bound in the reduced host under anhydrous conditions.²⁶ Similar studies on recombinant myoglobin have shown that the reduction of the heme cofactor can influence the acidity of nearby carboxylic acid

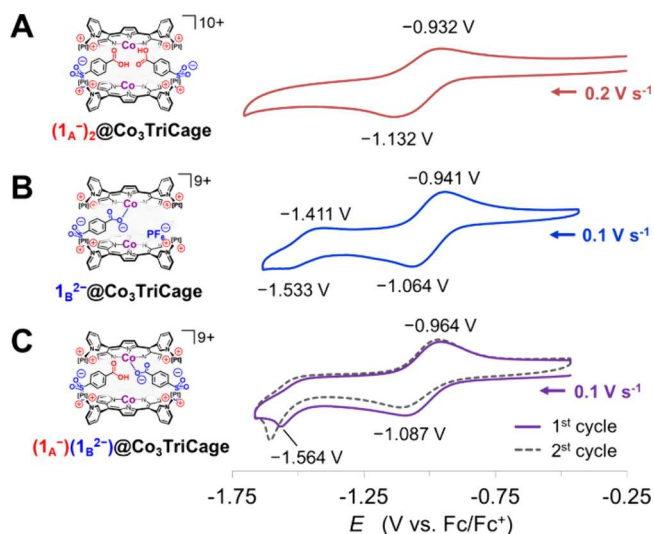


Figure 4. Cyclic voltammograms of (A) $(1_{\text{A}}^-)_2 @ \text{Co}_3\text{TriCage}$, (B) $1_{\text{B}}^{2-} @ \text{Co}_3\text{TriCage}$, and (C) $(1_{\text{A}}^-)(1_{\text{B}}^{2-}) @ \text{Co}_3\text{TriCage}$ recorded using a GCWE in MeCN containing 0.1 M TBAPF_6 .

residues, revealing notable electrostatic effects on the redox thermochemistry of heme proteins.^{4a} To our knowledge, such experiments have not previously been performed with artificial porous structures. Thus, our findings provide an unprecedented measurement of the thermodynamics of charging an artificial porous nanostructure with protons and electrons.²⁶ The complex $(1_{\text{A}}^-)(1_{\text{B}}^{2-}) @ \text{Co}_3\text{TriCage}$ also shows an extra cathodic feature that suggests the acidity of $(1_{\text{A}}^-)_2 @ \text{Co}_3\text{TriCage}$ is decreased considerably by reduction (Figure 4C). However, the change in acidity cannot reliably be estimated since the reduction feature is irreversible and changes in its exact appearance and position over multiple cycles.

Control experiments examined the CVs of 1:2 complexes between $\text{Co}_3\text{TriCage}$ and either $p\text{-tolylSO}_3^- (2^-)$ or 4-sulfanatomethylbenzoate (3^-). Both complexes show a single reversible reduction near -1 V vs $\text{Fc}^{+/\text{0}}$ (Figures S83, S84), confirming that the extra redox features near -1.5 V for complexes of 1_{B}^{2-} can be attributed to $\text{CO}_2^- \rightarrow \text{Co}^{\text{II}}$ coordination. Likewise, titration of $[\text{TBA}][\text{OAc}]$ into a 1 mM sample of $[(N\text{-methyl-3-pyridinium})_4\text{porphyrinCo}^{\text{II}}]^{4+}$ produced a gradual cathodic shift of the $\text{Co}^{\text{II}/\text{I}}$ redox couple, reaching a $\Delta E_{1/2}$ of -115 mV at a 50 mM concentration of acetate (Figure S85). This finding confirms that metal-carboxylate coordination alters the redox features of Co^{II} sites, while also revealing that this effect is much weaker outside the nanoconfined environment of $\text{Co}_3\text{TriCage}$.

^1H NMR spectroscopy was used to attempt to observe the diamagnetic *tris*- Co^{I} states of the host–guest complexes, as accessed via reduction of the host with Cp_2Co in CD_3CN . Addition of 2^- to $\text{Co}^{\text{I}}_3\text{TriCage}$ leads to the appearance of NMR signals consistent with strong, noncooperative 1:2 binding of this guest (Figure S88), similar to what we have reported for association of 2^- with unmetallated TriCage .^{11d} In contrast, reduction of $1_{\text{B}}^{2-} @ \text{Co}^{\text{I}}_3\text{TriCage}$ with 3 equiv Cp_2Co leads to a ^1H NMR spectrum matching that of empty $\text{Co}^{\text{I}}_3\text{TriCage}$,^{11c} with integration indicating significant precipitation of the host from solution (Figure S89). Thus, 1_{B}^{2-} appears to be ejected from the reduced host (Scheme 5), leading to partial precipitation of the host as seen for the other

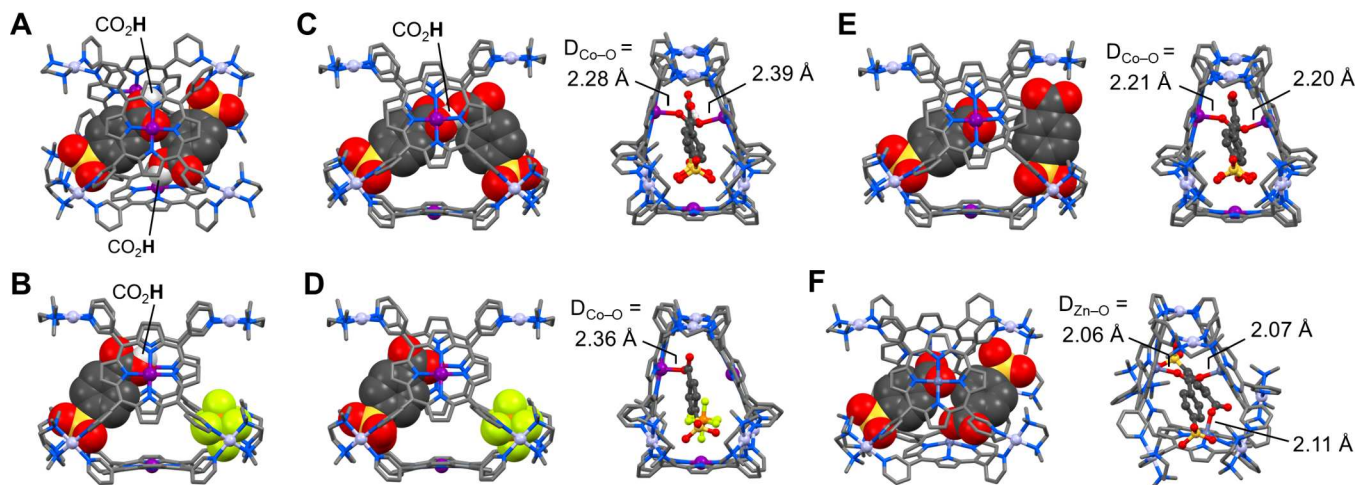
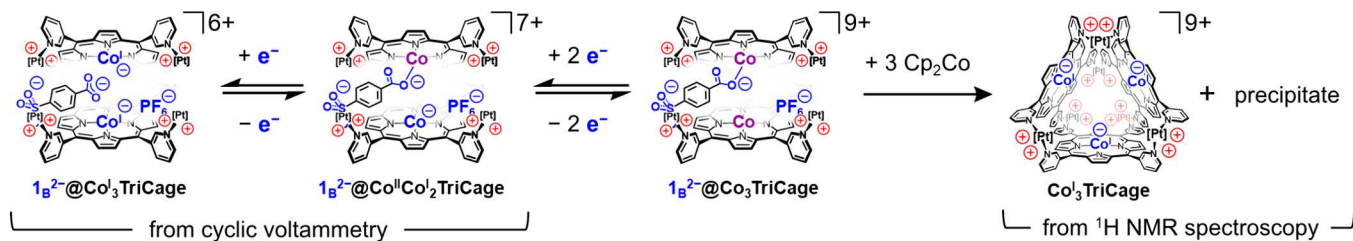
Scheme 5. Reduction of the 1:1 Complex 1_B^{2-} @ $\text{Co}_3\text{TriCage}$ as Observed by Cyclic Voltammetry and NMR Spectroscopy

Figure 5. Lowest energy computationally (DFT) optimized structures of (A) (1_A⁻)₂ @ Co₃TriCage, (B) (1_A⁻)(PF₆⁻) @ Co₃TriCage, (C) (1_A⁻)(1_B²⁻) @ Co₃TriCage, (D) (1_B²⁻)(PF₆⁻) @ Co₃TriCage, (E) (1_B²⁻)₂ @ Co₃TriCage, (F) (1_B²⁻)₂ @ Zn₃TriCage.

TriCages in the presence of excess 1_B²⁻. These findings are consistent with strong destabilization of the anionic CO₂⁻ group in the reduced state of the host.

The expulsion of an anionic group from Co^I₃TriCage is consistent with our previous observation that the reduction of free-base TriCage by 3 e⁻ induces the uptake of a cationic guest Cp₂Co⁺. Interestingly, however, this guest does not appear to bind in Co^I₃TriCage despite this cage having the same charge as (3e⁻)@TriCage. This discrepancy might be explained by the specific distribution of charge in the zwitterionic states of these hosts. Each electron added to TriCage is delocalized across the π* system of an entire porphyrin wall, representing a diffuse distribution of negative charge that might better complement a large cationic guest, while the concentration of negative charge near the center of Co^I₃TriCage would more strongly affect a charged group positioned near the middle of the host.

To provide another point of comparison for these effects, a new host Cu₃TriCage was prepared and examined. The paramagnetic ¹H NMR spectrum of Cu₃TriCage showed only a few signals, which were not affected by the binding of 1_A⁻ or 1_B²⁻ (Figures S53, S54). Nevertheless, it was possible to confirm the binding of these guests by ESI-MS (Figures S71, S72). Additionally, mixtures of Cu₃TriCage and 1_A⁻ partially protonate Et₂BnN (Figure S55), suggesting a similar or slightly weaker acidity when 1_A⁻ is bound in Cu₃TriCage vs Co₃TriCage. Thus, it is reasonable to assume that the CO₂⁻ group of 1_B²⁻ coordinates to Cu^{II}.

Interestingly, however, this interaction has only a weak influence on the reduction potentials of the copper–metalated cage. Empty Cu₃TriCage undergoes two quasireversible reductions at $E_{1/2} = -1.265$ and -1.588 V (Figure S86),

which are consistent with the two porphyrin π* reductions that are typical of copper-porphyrin complexes.²⁸ These reductions are shifted by at most -45 mV in the presence of 1_B²⁻ (Figure S87), revealing that the deprotonated guest has a weak effect on porphyrin-centered reductions, in contrast to the strong influence of 1_B²⁻ on one of the Co^{II}/Co^I reductions of Co₃TriCage. Thus, electrostatic interactions between 1_B²⁻ and the reduced M₃TriCages appear to be affected by the specific distribution of negative charge in the reduced hosts. However, without NMR spectroscopy to provide a more detailed understanding of host–guest interactions involving Cu₃TriCage in solution, we caution that conclusions drawn from studying this host are not as reliable as those from examining the Zn and Co derivatives.

Computational Optimization of Host–Guest Structures. It was not possible to obtain single-crystal X-ray diffraction data of sufficient quality to structurally characterize the complexes of 1_A⁻ and/or 1_B²⁻ in any of the TriCage derivatives, so computational analyses were employed to better understand how these guests sit inside the three hosts. Initial Hartree–Fock structural optimizations were followed by DFT optimizations (B3LYP functional,²⁹ 6-31++G** basis set for light atoms and LANL2DZ for metals³⁰), revealing 2 to 3 possible geometries for each complex containing two of the functional guests in any combination of protonation states (Figures 5 and S91 – S93). In all cases, the lowest energy structures agreed well with experimental results, providing additional insight into the origins of the host–guest and acid–base properties of these complexes.

For each host, the lowest energy (1_A⁻)₂ @ M₃TriCage structure has the SO₃⁻ groups of the two guests sitting along the edges of different porphyrin units (Figures 5A, S91E,

S93E), whereas smaller anions (e.g., PF_6^- , NO_3^-) tend to sit along opposite edges of the same porphyrin wall in experimentally determined structures of **TriCage** and related hosts.^{11a,d} Indeed, this latter anion placement was found upon optimizing complexes with one I_A^- and one PF_6^- guest (Figures 5B, S91A, S93A). It is likely that the less symmetric placement of the anions is favored in complexes with two I_A^- guests in order to accommodate the efficient packing of two lengthy benzoic acid units inside the hosts. In comparison, significantly higher energies (by 8–9 kcal mol⁻¹) were obtained for structures with a more symmetric placement of two I_A^- guests, even when this allows for hydrogen bonding between the guests (Figures S91C, S92C, S93C).

The lowest energy structures of the 1:1:1 complexes $(\text{I}_\text{A}^-)(\text{I}_\text{B}^{2-})@\text{M}_3\text{TriCage}$ are also similar across the three hosts, though in these cases the SO_3^- groups sit at opposite ends of a single porphyrin unit in order to accommodate hydrogen bonding between the guests^{19b,21} (Figures 5C, S91F, S93F). The resulting $\text{CO}_2\text{H} \cdots \text{O}_2\text{C}$ interactions are characterized by short O---O distances of 2.46–2.6 Å, representing strong hydrogen bonding^{5a} across the series of 1:1:1 complexes even though the CO_2^- group also coordinates to metal sites in the cobalt and zinc derivatives. Interestingly, the CO_2^- group bridges between two metal sites in these derivatives, while the optimized structures of the 1:1 complexes $\text{I}_\text{B}^{2-}@\text{M}_3\text{TriCage}$ have just a single oxygen atom coordinated to cobalt or zinc (Figures 5D and S93B). This difference may be the result of π - π interactions between the host and the additional I_A^- guest in the 1:1:1 complexes, which would reinforce the contraction of the host that is needed to facilitate a second metal–oxygen interaction. Regardless of the cause, the narrowed cavity and multiple stabilizing interactions of the CO_2^- and CO_2H groups might explain the experimental finding that $(\text{I}_\text{A}^-)(\text{I}_\text{B}^{2-})@\text{Co}_3\text{TriCage}$ has weaker interactions with water than found in other complexes of I_A^- or I_B^{2-} bound in **Co₃TriCage**.

In contrast to the monoprotic and diprotic states, the fully deprotonated complexes $(\text{I}_\text{B}^{2-})_2@\text{M}_3\text{TriCage}$ show different optimized structures for each host. In the cobalt version (Figure 5E), one of the I_B^{2-} guests maintains similar interactions with the host as seen in the 1:1:1 complex, including the bridging of the CO_2^- group between two Co^{II} sites. However, the second I_B^{2-} guest takes on a different binding mode in which its CO_2^- group is shifted away from the interior of the cage, interacting instead with one of the (tmada) Pt^{2+} units at one of the apertures of the host. Notably, this binding mode is seen for both of the I_B^{2-} guests in the optimized structure of $(\text{I}_\text{B}^{2-})_2@\text{TriCage}$ (Figure S91I), as expected based on the similar acidities of the 1:1:1 complexes in the unmetalated and cobalt–metalated hosts (see above). Lastly, $(\text{I}_\text{B}^{2-})_2@\text{Zn}_3\text{TriCage}$ has both CO_2^- groups coordinated to Zn^{II} sites (Figure 5F) consistent with the high acidities measured for both $(\text{I}_\text{A}^-)_2@\text{Zn}_3\text{TriCage}$ and $(\text{I}_\text{A}^-)(\text{I}_\text{B}^{2-})@\text{Zn}_3\text{TriCage}$ (see above). It is notable that the Zn^{II} sites are sufficiently electron withdrawing to allow the anionic carboxylate groups to sit only about 5.3 Å from each other (measured between the carbon atoms), whereas an analogous structure for $(\text{I}_\text{B}^{2-})_2@\text{Co}_3\text{TriCage}$ was found to be ~3.5 kcal mol⁻¹ higher in energy than the geometry with only one CO_2^- group coordinated to Co^{II} (Figures S92I,K).

The computational results described above correspond well to experimental findings even though hydration was neglected. However, since water has specific influences on the host–guest chemistry of the **M₃TriCages**, select complexes were

reoptimized with water molecules modeled explicitly (Figure 6). The complex $(\text{I}_\text{A}^-)_2@\text{Co}_3\text{TriCage}$ only has space for two

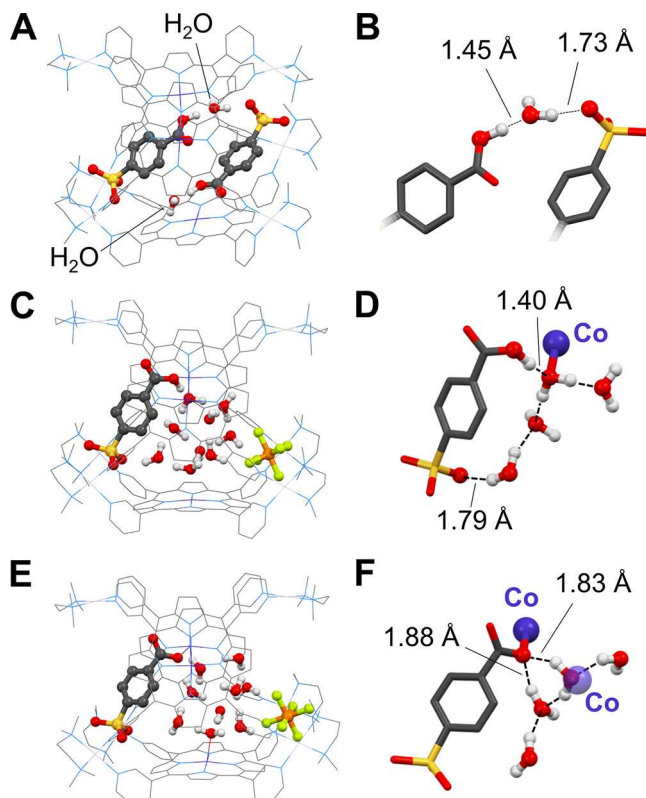


Figure 6. Computationally (DFT) optimized structures of hydrated host–guest complexes of I_A^- or I_B^{2-} bound in **Co₃TriCage**. (A) $(\text{I}_\text{A}^-)_2@\text{Co}_3\text{TriCage} \bullet 2\text{H}_2\text{O}$. (B) Expanded view of hydrogen bonding interactions between a water molecule and the two guests in $(\text{I}_\text{A}^-)_2@\text{Co}_3\text{TriCage} \bullet 2\text{H}_2\text{O}$. (C) $\text{I}_\text{A}^-@\text{Co}_3\text{TriCage} \bullet 9\text{H}_2\text{O}$. (D) Expanded view of water molecules interacting with the guest in $\text{I}_\text{A}^-@\text{Co}_3\text{TriCage} \bullet 9\text{H}_2\text{O}$. (E) $\text{I}_\text{B}^{2-}@\text{Co}_3\text{TriCage} \bullet 9\text{H}_2\text{O}$. (F) Expanded view of water molecules interacting with the guest in $\text{I}_\text{B}^{2-}@\text{Co}_3\text{TriCage} \bullet 9\text{H}_2\text{O}$. Note that 6D and 6F only display the four water molecules that differ in their hydrogen-bond connectivity between the complexes of I_A^- vs I_B^{2-} .

water molecules (Figure 6A), each of which acts as a hydrogen-bond acceptor to the CO_2H group of a different I_A^- guest. One of these water molecules also interacts with the sulfonate group of the opposite I_A^- guest to establish a $\text{CO}_2\text{H} \cdots \text{OH} \cdots \text{O}_3\text{S}$ hydrogen-bonding chain (Figure 6B), which likely explains why hydration promotes the cooperative binding of the two guests.

Hydrated states of $\text{I}_\text{A}^-@\text{Co}_3\text{TriCage}$ and $\text{I}_\text{B}^{2-}@\text{Co}_3\text{TriCage}$ were also optimized (Figures 6C–F). In both cases, a cluster of nine water molecules fits between the benzoic acid or benzoate guest and a PF_6^- anion bound at the opposite side of the cavity (Figures 6C,E). Five of the waters maintain similar hydrogen-bonding connectivity in both complexes, anchored by two hydrogen-bonding interactions with the PF_6^- anion as well as coordination of one water to the Co^{II} site nearest to the PF_6^- . The other four water molecules are affected more substantially by the protonation state of the guest (Figures 6D,F). In $\text{I}_\text{A}^-@\text{Co}_3\text{TriCage}$, one of these waters accepts a hydrogen bond from the CO_2H group of I_A^- , while another water acts as a hydrogen-bond donor to the SO_3^- group of the guest (Figure 6D). Conversely, in $\text{I}_\text{B}^{2-}@\text{Co}_3\text{TriCage}$, one of these waters acts as a hydrogen-bond acceptor to the CO_2H group of I_B^{2-} , while another water molecule acts as a hydrogen-bond donor to the SO_3^- group of the guest (Figure 6F).

Co₃TriCage, two waters act as hydrogen-bond donors to the anionic CO₂⁻ group of the guest without any waters interacting with the SO₃⁻ group (Figure 6F). The overall number of hydrogen-bonding interactions is maintained at 15 for both 1_A⁻@Co₃TriCage and 1_B²⁻@Co₃TriCage, which might help to explain why hydration does not appear to have a strong effect on stabilizing 1_B²⁻@Co₃TriCage relative to 1_A⁻@Co₃TriCage.

SUMMARY AND CONCLUSIONS

In summary, we have found that three M₃TriCage derivatives (M = H₂, Co, Zn) can bind 4-sulfanatobenzoic acid (1_A⁻) and/or its conjugate base (1_B²⁻) to form host–guest complexes containing up to two of these guests in any combination of protonation states. These complexes alter the pK_a of 1_A⁻ to a remarkable extent (pK_a = 12.75 to \geq 24.5), with the acidity of this guest increased by 8 orders of magnitude in (1_A⁻)₂@Zn₃TriCage and 4 orders of magnitude in (1_A⁻)₂@Co₃TriCage, while its acidity is decreased 4 orders of magnitude in the reduced complex 1_A⁻@Co^I₃TriCage. In comparison, unmetalated (1_A⁻)₂@TriCage increases the acidity of 1_A⁻ by just 2.5 pK_a units despite contributions from Coulombic effects and other factors (e.g., hydrogen bonding, pore hydration) that might be expected to increase the acidity of the guest. Thus, the M₃TriCages are distinguished by the dominant effects of the metal sites on altering acid–base chemistry.

In the most obvious effect, Lewis acidic Zn^{II} and Co^{II} ions increase the Brønsted acidity of 1_A⁻ by stabilizing its deprotonated state 1_B²⁻. In a more subtle corollary, CO₂⁻→Zn^{II} interactions withdraw enough electron density from 1_B²⁻ to stabilize two CO₂⁻ groups in close proximity, leading to relatively small changes of acidity for sequential deprotonation of two encapsulated 1_A⁻ guests. Conversely, the carboxylate group is destabilized by \sim 7 kcal mol⁻¹ in the reduced complex 1_B²⁻@Co^I₃TriCage due to Coulombic interactions with the anionic Co^I sites. This observation implies a large increase in the basicity of the encapsulated CO₂⁻ group, which is, to our knowledge, the first measurement of how a pore lined with redox-active metal sites^{11–13} can alter the thermodynamics of proton transfer. Similar behavior has been characterized in metalloproteins,^{4a} so these results establish an interesting parallel between the redox chemistry of Co₃TriCage and certain proteins.

Beyond fundamental novelty, these findings shed light on how porous materials might affect electrocatalytic processes. For example, the turnover frequencies of a number of important reactions can be influenced by the relative acidities of catalytic intermediates, proton relays, and the terminal source of H⁺,^{14a,b} so it is valuable to understand how porous nanostructures can be used to tune these thermodynamic relationships. From a different perspective, the ArCO₂⁻ guests are reminiscent of metal-bound CO₂⁻ intermediates that are often invoked in the reduction of CO₂.³¹ Our findings suggest that Lewis acidic metalloporphyrins may be especially useful for dissipating the charge of these intermediates in nanoconfined active sites.

Lastly, it is worth commenting on the interactions of water with Co₃TriCage and its complexes with 1_A⁻ and 1_B²⁻. Hydration of the host–guest complexes has a surprisingly weak influence on the acid–base equilibrium between these guests,^{3b–e} but it is still notable that both guests are readily hydrated inside the host, while empty Co₃TriCage has weak

interactions with water even in its zwitterionic tris-Co^I state (Figure S90). Since water is important for proton transport in confined environments,^{14c,32} these observations provide a mechanistic underpinning for the common observation^{12a,13a} that hydrophobic porphyrin nanomaterials favor CO₂ reduction over H⁺ reduction: if hydration of the active site is inhibited until a metal-bound CO₂⁻ intermediate forms, then H⁺ will not be able to access the reduced metal sites. However, we caution that more investigation is needed to better understand how hydration influences the electrochemical properties of the M₃TriCage, especially with respect to the kinetics of H⁺ transport. We are currently pursuing such studies.

ASSOCIATED CONTENT

Supporting Information

The Supporting Information is available free of charge at <https://pubs.acs.org/doi/10.1021/jacs.4c15873>.

Synthetic and experimental procedures; 1D and 2D NMR spectra (¹H, ¹³C{¹H}, COSY, ¹³C-¹H HSQC, and HMBC); ESI(+)-MS spectra; cyclic voltammograms; details of DFT calculations; and details of acid–base titration analyses (PDF)

AUTHOR INFORMATION

Corresponding Authors

Richard C. Remsing – Department of Chemistry and Chemical Biology, Rutgers, The State University of New Jersey, Piscataway, New Jersey 08854, United States;  orcid.org/0000-0002-0922-4882; Email: rick.remsing@rutgers.edu

Mark C. Lipke – Department of Chemistry and Chemical Biology, Rutgers, The State University of New Jersey, Piscataway, New Jersey 08854, United States;  orcid.org/0000-0003-0035-4565; Email: ml1353@chem.rutgers.edu

Authors

Taro J. Jones – Department of Chemistry and Chemical Biology, Rutgers, The State University of New Jersey, Piscataway, New Jersey 08854, United States

Kaitlyn G. Dutton – Department of Chemistry and Chemical Biology, Rutgers, The State University of New Jersey, Piscataway, New Jersey 08854, United States; Present Address: Department of Chemistry, Barnard College, Altschul Hall, 3009 Broadway, New York, New York 10027, United States;  orcid.org/0000-0002-3496-3425

Harendra S. Dhattarwal – Department of Chemistry and Chemical Biology, Rutgers, The State University of New Jersey, Piscataway, New Jersey 08854, United States;  orcid.org/0000-0001-6074-6734

P. Thomas Blackburn – Department of Chemistry and Chemical Biology, Rutgers, The State University of New Jersey, Piscataway, New Jersey 08854, United States

Rupak Saha – Department of Chemistry and Chemical Biology, Rutgers, The State University of New Jersey, Piscataway, New Jersey 08854, United States

Complete contact information is available at: <https://pubs.acs.org/10.1021/jacs.4c15873>

Author Contributions

T.J.J. and K.G.D. contributed equally to this work. All authors have given approval to the final version of the manuscript.

Notes

The authors declare no competing financial interest.

ACKNOWLEDGMENTS

M.C.L acknowledges the National Science Foundation (CHE award no. 2204045) for the financial support of this research. The authors also acknowledge Rutgers, The State University of New Jersey, for the financial support of this research, and the Office of Advanced Research Computing (OARC) at Rutgers, The State University of New Jersey, for providing access to the Amarel cluster and associated research computing resources. We thank Professor Mir Bowring of Reed College for making us aware of ref 23.

REFERENCES

- (1) (a) Grommet, A. B.; Feller, M.; Klajn, R. Chemical Reactivity Under Nanoconfinement. *Nat. Nanotechnol.* **2020**, *15*, 256–271. (b) Yoshizawa, M.; Klosterman, J. K.; Fujita, M. Functional Molecular Flasks: New Properties and Reactions within Discrete, Self-Assembled Hosts. *Angew. Chem., Int. Ed.* **2009**, *48*, 3418–3438. (c) Brown, C. J.; Toste, F. D.; Bergman, R. G.; Raymond, K. N. Supramolecular Catalysis in Metal-Ligand Cluster Hosts. *Chem. Rev.* **2015**, *115*, 3012–3035. (d) Bairagya, M. D.; Bujol, R. J.; Elgrishi, N. Fighting Deactivation: Classical and Emerging Strategies for Efficient Stabilization of Molecular Electrocatalysts. *Chem. - Eur. J.* **2019**, *26*, 3991–4000.
- (2) (a) Muñoz-Santiburcio, D.; Wittekindt, C.; Marx, D. Nanoconfinement Effects on Hydrated Excess Protons in Layered Materials. *Nat. Commun.* **2013**, *4*, 2349. (b) Muñoz-Santiburcio, D.; Marx, D. Chemistry in Nanoconfined Water. *Chem. Sci.* **2017**, *8*, 3444–3452. (c) Remsing, R. C.; McKendry, I. G.; Strongin, D. R.; Klein, M. L.; Zdilla, M. J. Frustrated Solvation Structures Can Enhance Electron Transfer Rates. *J. Phys. Chem. Lett.* **2015**, *6*, 4804–4808. (d) Bhullar, R. K.; Zdilla, M. J.; Klein, M. L.; Remsing, R. C. Effect of Water Frustration on Water Oxidation Catalysis in the Nanoconfined Interlayers of Layered Manganese Oxides Birnessite and Buserite. *J. Mater. Chem. A* **2021**, *9*, 6924–6932. (e) Dhattarwal, H. S.; Remsing, R. C.; Kashyap, H. K. Intercalation–Deintercalation of Water-in-Salt Electrolytes in Nanoscale Hydrophobic Confinement. *Nanoscale* **2021**, *13*, 4195–4205. (f) Bañuelos, J. L.; Borguet, E.; Brown, G. E.; Cygan, R. T.; DeYoreo, J. J.; Dove, P. M.; Gaigeot, M. P.; Geiger, F. M.; Gibbs, J. M.; Grassian, V. H.; Ilgen, A. G.; Jun, Y.; Kabengi, N.; Katz, L. E.; Kubicki, J. D.; Lützenkirchen, J.; Putnis, C. V.; Remsing, R. C.; Rosso, K. M.; Rother, G. Oxide– and Silicate–Water Interfaces and Their Roles in Technology and the Environment. *Chem. Rev.* **2023**, *123*, 6413–6544. (g) Ashbaugh, H. S.; Gibb, B. C.; Suating, P. Cavitand Complexes in Aqueous Solution: Collaborative Experimental and Computational Studies of the Wetting, Assembly, and Function of Nanoscopic Bowls in Water. *J. Phys. Chem. B* **2021**, *125*, 3253–3268.
- (3) (a) Churg, A. K.; Warshel, A. Control of the Redox Potential of Cytochrome and Microscopic Dielectric Effects in Proteins. *Biochemistry* **1986**, *25*, 1675–1681. (b) Urry, D. W.; Gowda, C.; Peng, S.; Parker, T. M.; Jing, N.; Harris, R. D. Nanometric Design of Extraordinary Hydrophobic-Induced pKa Shifts for Aspartic Acid: Relevance to Protein Mechanisms. *Biopolymers* **1994**, *34*, 889–896. (c) Isom, D. G.; Cannon, B. R.; Casteñeda, C. A.; Robinson, A.; García-Moreno, E. B. High Tolerance for Ionizable Residues in the Hydrophobic Interior of Proteins. *Proc. Natl. Acad. Sci. U.S.A.* **2008**, *105*, 17784–17788. (d) Isom, D. G.; Casteñeda, C. A.; Cannon, B. R.; García-Moreno, E. B. Large Shifts in pKa values of Lysin Residues Buried Inside a Protein. *Proc. Natl. Acad. Sci. U.S.A.* **2011**, *108*, 5260–5265. (e) Dwyer, J. J.; Gittis, A. G.; Karp, D. A.; Lattman, E. E.; Spencer, D. S.; Stites, W. E.; García-Moreno, E. B. High Apparent Dielectric Constants in the Interior of a Protein Reflect Water Penetration. *Biophys. J.* **2000**, *79*, 1610–1620.
- (4) (a) Varadarajan, R.; Zewert, T. E.; Gray, H. B.; Boxer, S. G. Effects of Buried Ionizable Amino Acids on the Reduction Potential of Recombinant Myoglobin. *Science* **1989**, *243*, 69–72. (b) Westheimer, F. H. Coincidences, Decarboxylation, and Electrostatic Effects. *Tetrahedron* **1995**, *51*, 3–20. (c) Warshel, A.; Sharma, P. K.; Kato, M.; Xiang, Y.; Liu, H.; Olsson, M. H. M. Electrostatic Basis for Enzyme Catalysis. *Chem. Rev.* **2006**, *8*, 3210–3235. (d) Pinitglang, S.; Watts, A. B.; Patel, M.; Reid, J. D.; Noble, M. A.; Gul, S.; Bokth, A.; Naeem, A.; Patel, H.; Thomas, E. W.; Sreedharan, S. K.; Verma, C.; Brocklehurst, K. A Classical Enzyme Active Center Motif Lacks Catalytic Competence until Modulated Electrostatically. *Biochemistry* **1997**, *36*, 9968–9982.
- (5) (a) Cleland, W. W.; Frey, P. A.; Gertl, J. A. The Low Barrier Hydrogen Bond in Enzymatic Catalysis. *J. Biol. Chem.* **1998**, *273*, 25529–25532. (b) Ha, N.-C.; Kim, M.-S.; Lee, W.; Choi, K. Y.; Oh, B.-H. Detection of Large pKa Perturbations of an Inhibitor and a Catalytic Group at an Enzyme Active Site, a Mechanistic Basis for Catalytic Power of Many Enzymes. *J. Biol. Chem.* **2000**, *275*, 41100–41106. (c) Thurlkill, R. L.; Grimsley, G. R.; Scholtz, J. M.; Pace, C. N. Hydrogen Bonding Markedly Reduces the pK of Buried Carboxyl Groups in Proteins. *J. Mol. Biol.* **2006**, *362*, 594–604.
- (6) (a) Pluth, M. D.; Bergman, R. G.; Raymond, K. N. Making Amines Strong Bases: Thermodynamic Stabilization of Protonated Guests in a Highly-Charged Supramolecular Host. *J. Am. Chem. Soc.* **2007**, *129*, 11459–11467. (b) Pluth, M. D.; Bergman, R. G.; Raymond, K. N. Acid Catalysis in Basic Solution: A Supramolecular Host Promotes Orthoformate Hydrolysis. *Science* **2007**, *316*, 85–88. (c) Hong, C. M.; Morimoto, M.; Kapustin, E. A.; Alzakhem, N.; Bergman, R. G.; Raymond, K. N.; Toste, F. D. Deconvoluting the Role of Charge in a Supramolecular Catalyst. *J. Am. Chem. Soc.* **2018**, *140*, 6591–6595. (d) Murase, T.; Nishijima, Y.; Fujita, M. Cage-Catalyzed Knoevenagel Condensation under Neutral Conditions in Water. *J. Am. Chem. Soc.* **2012**, *134*, 162–164. (e) Cullen, W.; Misuraca, M. C.; Hunter, C. A.; Williams, N. H.; Ward, M. D. Highly Efficient Catalysis of the Kemp Elimination in the Cavity of a Cubic Coordination Cage. *Nat. Chem.* **2016**, *8*, 231–236. (f) Cullen, W.; Metherell, A. J.; Wragg, A. B.; Taylor, C. G. P.; Williams, N. H.; Ward, M. D. Catalysis in a Cationic Coordination Cage Using a Cavity-Bound Guest and Surface-Bound Anions: Inhibition, Activation, and Autocatalysis. *J. Am. Chem. Soc.* **2018**, *140*, 2821–2828. (g) Ngai, C.; Wu, H.-T.; da Camara, B.; Williams, C. G.; Mueller, L. J.; Julian, R. R.; Hooley, R. J. Moderated Basicity of Endohedral Amine Groups in an Octa-Cationic Self-Assembled Cage. *Angew. Chem., Int. Ed.* **2022**, *61*, No. e202117011. (h) Cullen, W.; Thomas, K. A.; Hunter, C. A.; Ward, M. D. pH-Controlled Selection Between One of Three Guests from a Mixture Using a Coordination Cage Host. *Chem. Sci.* **2015**, *6*, 4025–4028.
- (7) (a) Wang, K.; Cai, X.; Yao, W.; Tang, D.; Kataria, R.; Ashbaugh, H. S.; Byers, L. D.; Gibb, B. C. Electrostatic Control of Macrocyclization Reactions within Nanospaces. *J. Am. Chem. Soc.* **2019**, *141*, 6740–6747. (b) Cai, X.; Kataria, R.; Gibb, B. C. Intrinsic and Extrinsic Control of the pKa of Thiol Guests Inside Yoctoliter Containers. *J. Am. Chem. Soc.* **2020**, *142*, 8291–8298. (c) Zhang, Q.; Tiefenbacher, K. Terpene Cyclization Catalyzed Inside a Self-Assembled Cavity. *Nat. Chem.* **2015**, *7*, 197–202.
- (8) (a) Száraz, S.; Oesterhelt, D.; Ormos, P. pH-induced structural changes in bacteriorhodopsin studied by Fourier transform infrared spectroscopy. *Biophys. J.* **1994**, *57*, 1706–1712. (b) Luecke, H.; Richter, H.-T.; Lanyi, J. K. Proton Transfer Pathways in Bacteriorhodopsin at 2.3 Angstrom Resolution. *Science* **1998**, *280*, 1934–1937.
- (9) (a) Karp, D. A.; Gittis, A. G.; Stahley, M. R.; Fitch, C. A.; Stites, W. E.; García-Moreno, E. B. High Apparent Dielectric Constant Inside a Protein Reflects Structural Reorganization Coupled to the Ionization of an Internal Asp. *Biophys. J.* **2007**, *92*, 2041–2053. (b) Harms, M. J.; Casteñeda, C. A.; Schlessman, J. L.; Sue, G. R.; Isom, D. G.; Cannon, B. R.; García-Moreno, E. B. The pKa Values of Acidic and Basic Residues Buried at the Same Internal Location in a Protein Are Governed by Different Factors. *J. Mol. Biol.* **2009**, *389*,

34–47. (c) Grimsley, G. R.; Scholtz, J. M.; Pace, C. N. A summary of the measured pK values of the ionizable groups in folded proteins. *Protein Sci.* **2009**, *18*, 247–251. (d) Awoonor-Williams, E.; Golosov, A. A.; Hornak, V. Benchmarking *In Silico* Tools for Cysteine pKa Prediction. *J. Chem. Inf. Model.* **2023**, *63*, 2170–2180.

(10) (a) Cook, T. R.; Stang, P. J. Recent Developments in the Preparation and Chemistry of Metallacycles and Metallacages via Coordination. *Chem. Rev.* **2015**, *115*, 7001–7045. (b) Durot, S.; Taesch, J.; Heitz, V. Multiporphyrinic Cages: Architectures and Functions. *Chem. Rev.* **2014**, *114*, 8542–8578. (c) Fujita, N.; Biradha, K.; Fujita, M.; Sakamoto, S.; Yamaguchi, K. A Porphyrin Prism: Structural Switching Triggered by Guest Inclusion. *Angew. Chem., Int. Ed.* **2001**, *40*, 1718–1721. (d) Bar, A. K.; Mohapatra, S.; Zangrandi, E.; Mukherjee, P. S. A Series of Trifacial Pd₆ Molecular Barrels with Porphyrin Walls. *Chem. - Eur. J.* **2012**, *18*, 9571–9579.

(11) (a) Dutton, K. G.; Rothschild, D. A.; Pastore, D. B.; Emge, T. J.; Lipke, M. C. The Influence of Redox-Active Linkers on the Stability and Physical Properties of a Highly Electroactive Porphyrin Nanoprism. *Inorg. Chem.* **2020**, *59*, 12616–12624. (b) Mansoor, Iram F.; Dutton, K. G.; Rothschild, D. A.; Remsing, R. C.; Lipke, M. C. Uptake, Trapping, and Release of Organometallic Cations by Redox-Active Cationic Hosts. *J. Am. Chem. Soc.* **2021**, *143*, 16993–17003. (c) Blackburn, P. Thomas; Mansoor, Iram F.; Dutton, Kaitlyn G.; Tyryshkin, Alexei M.; Lipke, Mark C. Accessing three oxidation states of cobalt in M₆L₃ nanoprisms with cobalt–porphyrin walls. *Chem. Commun.* **2021**, *57*, 11342–11345. (d) Dutton, K. G.; Jones, T. J.; Emge, T. J.; Lipke, M. C. Cage Match: Comparing the Anion Binding Ability of Isostructural Versus Isofunctional Pairs of Metal–Organic Nanocages. *Chem.—Eur. J.* **2024**, *30*, No. e202303013. (e) Blackburn, P. Thomas; Lipke, Mark C. Effects of a triangular nanocage structure on the binding of neutral and anionic ligands to Co^{II} and Zn^{II} porphyrins. *J. Coord. Chem.* **2022**, *75*, 1520–1542.

(12) (a) Smith, P. T.; Benke, B. P.; Cao, Z.; Kim, Y.; Nichols, E. M.; Kim, K.; Chang, C. J. Iron Porphyrins Embedded into a Supramolecular Porous Organic Cage for Electrochemical CO₂ Reduction in Water. *Angew. Chem., Int. Ed.* **2018**, *57*, 6984–6988. (b) Smith, P. T.; Kim, Y.; Benke, B. P.; Kim, K.; Chang, C. J. Supramolecular Tuning Enables Selective Oxygen Reduction Catalyzed by Cobalt Porphyrins for Direct Electrosynthesis of Hydrogen Peroxide. *Angew. Chem., Int. Ed.* **2020**, *59*, 4902–4907. (c) Oldacre, A. N.; Friedman, A. E.; Cook, T. R. A Self-Assembled Cofacial Cobalt Porphyrin Prism for Oxygen Reduction Catalysis. *J. Am. Chem. Soc.* **2017**, *139*, 1424–1427. (d) Crawley, M. R.; Zhang, D.; Oldacre, A. N.; Beavers, C. M.; Friedman, A. E.; Cook, T. R. Tuning the Reactivity of Cofacial Porphyrin Prisms for Oxygen Reduction Using Modular Building Blocks. *J. Am. Chem. Soc.* **2021**, *143*, 1098–1106. (e) Crawley, M. R.; Zhang, D.; Cook, T. R. Electrocatalytic production of hydrogen peroxide enabled by post-synthetic modification of a self-assembled porphyrin cube. *Inorg. Chem. Front.* **2022**, *10*, 316–324. (f) Nurtila, S. S.; Zaffaroni, R.; Mathew, S.; Reek, J. N. H. Control of the overpotential of a [FeFe] hydrogenase mimic by a synthetic second coordination sphere. *Chem. Commun.* **2019**, *55*, 3081–3084.

(13) (a) Lin, S.; Diercks, C. S.; Zhang, Y.-B.; Kornienko, N.; Nichols, E. M.; Zhao, Y.; Paris, A. R.; Kim, D.; Yang, P.; Yaghi, O. M.; Chang, C. J. Covalent organic frameworks comprising cobalt porphyrins for catalytic CO₂ reduction in water. *Science* **2015**, *349*, 1208–1213. (b) Kornienko, N.; Zhao, Y.; Kley, C. S.; Zhu, C.; Kim, D.; Lin, S.; Chang, C. J.; Yaghi, O. M.; Yang, P. Metal–Organic Frameworks for Electrocatalytic Reduction of Carbon Dioxide. *J. Am. Chem. Soc.* **2015**, *137*, 14129–14135. (c) Liberman, I.; Shimoni, R.; Ifraimov, R.; Rozenberg, I.; Singh, C.; Hod, I. Active-Site Modulation in an Fe-Porphyrin-Based Metal–Organic Framework through Ligand Axial Coordination: Accelerating Electrocatalysis and Charge-Transport Kinetics. *J. Am. Chem. Soc.* **2020**, *142*, 1933–1940. (d) Shimoni, R.; Shi, Z.; Binyamin, S.; Yang, Y.; Liberman, I.; Ifraimov, R.; Mukhopadhyay, S.; Zhang, L.; Hod, I. Electrostatic Secondary-Sphere Interactions That Facilitate Rapid and Selective Electrocatalytic CO₂ Reduction in a Fe-Porphyrin-Based Metal–Organic Framework. *Angew. Chem., Int. Ed.* **2022**, *61*, No. e202206085. (e) Gong, L.; Chen, B.; Gao, Y.; Yu, B.; Wang, Y.; Han, B.; Lin, C.; Bian, Y.; Qi, D.; Jiang, J. Covalent organic frameworks based on tetraphenyl-p-phenylenediamine and metallocporphyrin for electrochemical conversion of CO₂ to CO. *Inorg. Chem. Front.* **2022**, *9*, 3217–3223. (f) Wu, Q.-J.; Si, D.-H.; Wu, Q.; Dong, Y.-L.; Cao, R.; Huang, Y.-B. Boosting Electrocatalysis of CO₂ over Cationic Covalent Organic Frameworks: Hydrogen Bonding Effects of Halogen Ions. *Angew. Chem., Int. Ed.* **2023**, *62*, No. e202215687.

(14) (a) Teinl, K.; Patrick, B. O.; Nichols, E. M. Linear Free Energy Relationships and Transition State Analysis of CO₂ Reduction Catalysts Bearing Second Coordination Spheres with Tunable Acidity. *J. Am. Chem. Soc.* **2023**, *145* (31), 17176–17186. (b) Sonea, A.; Crudo, N. R.; Warren, J. J. Understanding the Interplay of the Brønsted Acidity of Catalyst Ancillary Groups and the Solution Components in Iron-porphyrin-Mediated Carbon Dioxide Reduction. *J. Am. Chem. Soc.* **2024**, *146*, 3721–3731. (c) Yeh, C.-Y.; Chang, C. J.; Nocera, D. G. Hangman” Porphyrins for the Assembly of a Model Heme Water Channel. *J. Am. Chem. Soc.* **2001**, *7*, 1513–1514. (d) Bediako, D. K.; Solis, B. H.; Dogutan, D. K.; Roubelakis, M. M.; Maher, A. G.; Lee, C. H.; Chambers, M. B.; Hammes-Schiffer, S.; Nocera, D. G. Role of pendant proton relays and proton-coupled electron transfer on the hydrogen evolution reaction by nickel hangman porphyrins. *Proc. Natl. Acad. Sci. U.S.A.* **2014**, *111*, 15001–15006.

(15) To our knowledge, the largest changes of acidity measured in proteins are $\Delta pK_a \approx 8.5$ (see references ^{8a,9c,d}), while pK_a changes of ≤ 6 are more common in both proteins and artificial nanocages (see references ^{3b,4b,5b,6,7a,b,9}).

(16) Craen, D. V.; Kalarikkal, M. G.; Holstein, J. J. A Charge-Neutral Self-Assembled L₂Zn₂ Helicate as Bench-Stable Receptor for Anion Recognition at Nanomolar Concentration. *J. Am. Chem. Soc.* **2022**, *144*, 18135–18143.

(17) Bryant, R. G. The NMR time scale. *J. Chem. Educ.* **1983**, *60*, 933–935.

(18) ¹³C{¹H} NMR and 2D NMR experiments were used to confirm the assignments of the signals of the 1_A⁻ guests in the TriCages. These experiments required high sample concentrations and the use of non-routine (700 MHz) NMR instrumentation, which was prohibitive for characterizing all the complexes, so (1_A⁻)₂@Zn₃TriCage was selected for representative characterization (see Figures S39 – S43). The chemical shifts of the ¹H NMR signals of the guest are similar to those reported for p-tolylSO₃⁻ in TriCage (reference 11d), which has the CH₃ group placed near the center of the host.

(19) (a) Tshepelevitsh, S.; Kütt, A.; Lõkov, M.; Kaljurand, I.; Saame, J.; Heering, A.; Plieger, P. G.; Vianello, R.; Leito, I. On the Basicity of Organic Bases in Different Media. *Eur. J. Org. Chem.* **2019**, *2019*, 6735–6748. (b) Kütt, A.; Tshepelevitsh, S.; Saame, J.; Lõkov, M.; Kaljurand, I.; Selberg, S.; Leito, I. Strengths of Acids in Acetonitrile. *Eur. J. Org. Chem.* **2021**, *2021*, 1407–1419. (c) Kaupmees, K.; Kaljurand, I.; Leito, I. Influence of Water Content on the Acidities in Acetonitrile. Quantifying Charge Delocalization in Anions. *J. Phys. Chem. A* **2010**, *114*, 11788–11793.

(20) (a) Patrick, S. C.; Beer, P. D.; Davis, J. J. Solvent effects in anion recognition. *Nat. Rev. Chem.* **2024**, *8*, 256–276. (b) Sokkalingam, P.; Shrberg, J.; Rick, S. W.; Gibb, B. C. Binding Hydrated Anions with Hydrophobic Pockets. *J. Am. Chem. Soc.* **2016**, *138*, 48–51.

(21) Fourmond, V.; Jacques, P.-A.; Fontecave, M.; Artero, V. H₂ Evolution and Molecular Electrocatalysts: Determination of Overpotentials and Effect of Homoconjugation. *Inorg. Chem.* **2010**, *49*, 10338–10347.

(22) Traces of water can have relatively large effects on increasing the acidity of benzoic acids in MeCN (see reference 19c), so it is worth noting that our measured pK_a (20.75 ± 0.04) for 4-sulfatobenzoic acid (1_A⁻) is reasonable based on the known acidity of benzoic acid in MeCN (pK_a = 21.5, reference 19b) and the positive σ_p Hammett parameter for SO₃⁻ (reference 23). Additionally, even a somewhat large systematic error (≤ 1.5 pK_a units) in the acidity of 1_A⁻

measured in bulk MeCN would not affect our conclusions about the relative contributions of different factors that influence the acidity of this guest inside the $M_3\text{TriCages}$.

(23) Hansch, C.; Leo, A.; Taft, R. W. A Survey of Hammett Substituent Constants and Resonance and Field Parameters. *Chem. Rev.* **1991**, *91*, 165–195.

(24) A statistical correction of + 0.3 units should be applied to the pK_a of $(1_A^-)_2@\text{Co}_3\text{TriCage}$ when comparing the acidity of this diprotic complex with that of the monoprotic complex $1_A^-@\text{Co}_3\text{TriCage}$. Thus, the acidity of the latter complex relative to the former is appropriately estimated as $\Delta pK_a \leq -0.83 \pm 0.16$.

(25) The acidities of $(1_A^-)_2@\text{Co}_3\text{TriCage}$ under hydrated vs. anhydrous conditions are not statistically distinguishable based on direct pK_a measurements, but the stronger interactions of water with $(1_A^-)_2@\text{Co}_3\text{TriCage}$ vs. $(1_A^-)(1_B^{2-})@\text{Co}_3\text{TriCage}$ make it clear that the hydrated state of the diprotic complex must be at least slightly less acidic than its anhydrous state.

(26) Agarwal, R. G.; Coste, S. C.; Groff, B. D.; Heuer, A. M.; Noh, H.; Parada, G. A.; Wise, C. F.; Nichols, E. M.; Warren, J. J.; Mayer, J. M. Free Energies of Proton-Coupled Electron Transfer Reagents and Their Applications. *Chem. Rev.* **2022**, *122*, 1–49.

(27) The strength of $\text{CO}_2^- \rightarrow \text{Co}^{II}$ coordination in anhydrous $1_B^{2-}@\text{Co}_3\text{TriCage}$ was determined to be ca. 4 kcal mol⁻¹ based on comparisons of pK_a values that indicate an enhancement of stability of the dianion by ~ 2.3 kcal mol⁻¹ in this complex relative to $(1_A^-)(1_B^{2-})@\text{TriCage}$, and the estimate that $1_A^- \cdots 1_B^{2-}$ hydrogen bonding stabilizes the latter complex by ~ 1.5 kcal mol⁻¹. Thus, the $\text{CO}_2^- \rightarrow \text{Co}^{II}$ interaction can be approximated as 2.3 + 1.5 kcal mol⁻¹.

(28) Ye, L.; Ou, Z.; Fang, Y.; Xue, S.; Song, Y.; Wang, L.; Wang, M.; Kadish, K. M. Electrochemistry of nonplanar copper(II) tetrabutano- and tetrabenzotetraarylporphyrins in nonaqueous media. *RSC Adv.* **2015**, *5*, 77088–77096.

(29) (a) Becke, A. D. Density-Functional Exchange-Energy Approximation with Correct Asymptotic Behavior. *Phys. Rev. A* **1988**, *38*, 3098–3100. (b) Lee, C. T.; Yang, W. T.; Parr, R. G. Development of the Colle-Salvetti Correlation-Energy Formula into a Functional of the Electron Density. *Phys. Rev. B* **1988**, *37*, 785–789.

(30) (a) Petersson, G. A.; Al-Laham, M. L. A complete basis set model chemistry. II. Open-shell systems and the total energies of the first-row atoms. *J. Chem. Phys.* **1991**, *94*, 6081–6090. (b) Hay, P. J.; Wadt, W. R. *Ab initio* effective core potentials for molecular calculations – potentials for the transition-metal atoms Sc to Hg. *J. Chem. Phys.* **1985**, *82*, 270–283.

(31) (a) Shen, J.; Kolb, M. J.; Göttle, A. J.; Koper, M. T. DFT Study on the Mechanism of the Electrochemical Reduction of CO_2 Catalyzed by Cobalt Porphyrins. *J. Phys. Chem. C* **2016**, *120*, 15714–15721. (b) Zhu, C.; D'Agostino, C.; de Visser, S. P. CO_2 Reduction by an Iron(I) Porphyrinate System: Effect of Hydrogen Bonding on the Second Coordination Sphere. *Inorg. Chem.* **2024**, *63*, 4474–4481.

(32) (a) Can, M.; Armstrong, F. A.; Ragsdale, S. W. Structure, Function, and Mechanism of the Nickel Metalloenzymes, CO Dehydrogenase, and Acetyl-CoA Synthase. *Chem. Rev.* **2014**, *114*, 4149–4174. (b) Hussein, R.; Graca, A.; Forsman, J.; Aydin, A. O.; Hall, M.; Gaetcke, J.; Chernev, P.; Wendler, P.; Dobbek, H.; Messinger, J.; Zouni, A.; Schröder, W. P. Cryo-electron microscopy reveals hydrogen positions and water networks in photosystem II. *Science* **2024**, *384*, 1349–1355. (c) Hart-Cooper, W. M.; Sgarlata, C.; Perrin, C. L.; Toste, F. D.; Bergman, R. G.; Raymond, K. N. Protein-like proton exchange in a synthetic host cavity. *Proc. Natl. Acad. Sci. U.S.A.* **2015**, *112*, 15303–15307.